Journal of
Materials Chemistry B

REVIEW

Check for updates

Cite this: J. Mater. Chem. B, 2017, 5, 7444

Visualizing molecular distributions for biomaterials applications with mass spectrometry imaging: a review

Martin R. L. Paine, †[ab] Pieter C. Kooijman, †[ac] Gregory L. Fisher, [d] Ron M. A. Heeren, [a] Facundo M. Fernández [bef] and Shane R. Ellis *[a]

Received 21st April 2017,
Accepted 11th August 2017

DOI: 10.1039/c7tb01100h

rsc.li/materials-b

Mass spectrometry imaging (MSI) is a rapidly emerging field that is continually finding applications in new and exciting areas. The ability of MSI to measure the spatial distribution of molecules at or near the surface of complex substrates makes it an ideal candidate for many applications, including those in the sphere of materials chemistry. Continual development and optimization of both ionization sources and analyzer technologies have resulted in a wide array of MSI tools available, both commercially available and custom-built, with each configuration possessing inherent strengths and limitations. Despite the unique potential of MSI over other chemical imaging methods, their potential and application to (bio)materials science remains in our view a largely underexplored avenue. This review will discuss these techniques enabling high parallel molecular detection, focusing on those with reported uses in (bio)materials chemistry applications and highlighted with select applications. Different technologies are presented in three main sections; secondary ion mass spectrometry (SIMS) imaging, matrix-assisted laser desorption ionization (MALDI) MSI, and emerging MSI technologies with potential for biomaterial analysis. The first two sections (SIMS and MALDI) discuss well-established methods that are continually evolving both in technological advancements and in experimental versatility. In the third section, relatively new and versatile technologies capable of performing measurements under ambient conditions will be introduced, with reported applications in materials chemistry or potential applications discussed. The aim of this review is to provide a concise resource for those interested in utilizing MSI for applications such as biomimetic materials, biological/synthetic material interfaces, polymer formulation and bulk property characterization, as well as the spatial and chemical distributions of nanoparticles, or any other molecular imaging application requiring broad chemical speciation.

Introduction

Interactions at the surface of biomaterials have a major impact on their *in vivo* performance and physiological response of the host. Therefore, detailed characterization of surface properties, both physical and chemical, is required to engineer new materials and increase their biocompatibility.[1,2] Many analytical techniques have been routinely employed to characterize the surface properties of biomaterials including but not limited to; X-ray photoelectron spectroscopy (XPS),[3] atomic force microscopy (AFM),[4] Auger electron spectroscopy (AES),[5] contact angle methods,[6] vibrational spectroscopy (*e.g.*, Raman and Fourier transform infrared spectroscopy),[7] near edge X-ray absorption fine structure (NEXAFS)[8] and energy dispersive X-ray spectroscopy (EDX).[9] An informative comparison between these and MS-based approaches is provided in a review by Senoner and Unger.[10] Of the aforementioned techniques, detailed elemental and topographical information of the surface can be obtained, but this information usually relates to one or a few chemical species, lacking specific chemical information at the molecular level. With the exception of vibrational spectroscopy, complementary imaging techniques are typically required when broadband molecular information from both the substrate and the biological material that interacts with the substrate is desired.

[a] *M4I, The Maastricht MultiModal Molecular Imaging Institute, Maastricht University, Maastricht 6229 ER, The Netherlands. E-mail: s.ellis@maastrichtuniversity.nl*
[b] *School of Chemistry and Biochemistry, Georgia Institute of Technology, Atlanta, GA 30332, USA*
[c] *TI-COAST, Amsterdam 1098 XH, The Netherlands*
[d] *Physical Electronics, Inc., Chanhassen, Minnesota 55317, USA*
[e] *Integrated Cancer Research Center, Georgia Institute of Technology, Atlanta, GA 30332, USA*
[f] *Institute of Bioengineering and Biosciences, Georgia Institute of Technology, Atlanta, GA 30332, USA*
† Authors contributed equally.

Mass spectrometry imaging (MSI) enables visualization of a broad range of chemical species in a single experiment with high molecular specificity and the ability to structurally characterize detected molecules. As many materials chemistry applications have traditionally focused on the analysis of inorganic or covalently bound materials with high (<1 μm) spatial resolution, secondary ion mass spectrometry (SIMS) has been a mainstay for chemical imaging of materials in many disciplines as it is particularly well suited for such analyses.[10–13] However, as research into biomaterials and their associated biomolecular interactions has emerged, so too has the demand for new MSI methods enabling detection and characterization of many classes of labile biomolecules. With the development of alternative ionization methods and rapid improvements in MSI instrumentation, both in terms of mass analyzer and sampling/ionization technologies, massive gains in mass-resolving power, speed and sensitivity have been achieved. These dramatic improvements have positioned MSI as a unique resource within a growing number of analytical facilities. In particular, the use of MSI for the investigation of biological tissues has flourished, providing a wealth of information on the spatial distribution of pharmaceuticals, metabolites, lipids, peptides, and proteins from practically every type of organic substrate.[14–16] The increased usage of MSI for biomolecular investigations has resulted in successful methodologies for a broad family of compound classes, making the translation to inorganic or non-biological substrates a logical step. Thus, emerging fields such as biomaterial development, where changes in surface composition and structure of synthetic materials placed inside the body (*e.g.*, biomimetics or biomedical devices) affect a biological response are primed for interrogation by MSI. As a surface sampling technique, MSI is well equipped to probe biomaterials that encompass this interface between synthetic substrates and biological tissue.[17,18] Characterizing the biomaterial surface properties (*i.e.*, chemical composition, structure, orientation) and understanding the biological effect these properties have by measuring biomolecules on these surfaces is paramount to the development of biomaterial technology.

The ability to perform MSI for a particular application depends largely on the type of desorption/ionization source employed of which there are three major categories; secondary ion mass spectrometry (SIMS), matrix-assisted laser desorption/ionization (MALDI), and various ambient mass spectrometric methods. Each technique is capable of producing ions in both positive- and negative-ion mode (broadly referring to detection of basic and acidic compounds, respectively), however their method of operation varies significantly leading to different populations of ions detected. SIMS represents the most energetic desorption technique, capable of ablating covalently or ionically bound material and penetrating into the depth of the substrate, making it well suited for elemental and inorganic analyses. MALDI is a softer desorption technique, capable of desorbing and ionizing loosely bound inorganic material and a wide range of biomolecules (proteins, peptides, lipids, and metabolites). Ambient techniques generally represent the softest desorption techniques and are best suited to delicate substrates (particularly those not vacuum stable) and labile organic molecules in the 50–2000 Da range. Therefore, alternative MSI techniques such as MALDI and ambient methods may be more effective in biomaterial applications where broader chemical detection is required or when probing delicate substrates.

In this review, we highlight the broad array of MSI techniques currently available for molecular detection by showcasing their reported use in biomaterial applications, as well as broader materials science applications to illustrate the potential of these techniques for future research. The discussion includes concise descriptions of the processes underpinning each technique, current developments in instrumentation technology, and key applications that exemplify the benefit of MSI for biomaterial surface analysis. Finally, a perspective on the role of new MSI approaches at the intersection of biomaterial analysis is provided.

Secondary ion mass spectrometry (SIMS)

SIMS was the first MS technique employed for imaging and arguably the one most familiar to materials scientists.[11,19,20] SIMS utilizes the release of charged (ionized) material from a substrate upon impact of an electrostatically focused high-energy primary ion beam (traditionally from monoatomic sources such as Au^+, Ga^+ and In^+). As the high-energy (10–40 keV) primary ions impact the surface, a collisional cascade is initiated in the top few monolayers of the sample, leading to the ejection of secondary particles consisting of sputtered neutral molecules, ions, molecular fragments (of both neutrals and ions), and electrons.[21,22] The secondary ions generated, typically protonated/deprotonated ions, cationized adducts or radicals, are then detected based on their mass-to-charge ratio (m/z), typically using time-of-flight (ToF) mass spectrometry. For SIMS analyses, samples are typically mounted in a high vacuum sample chamber, must be as flat as possible and be mounted onto conductive substrates to minimize the effect of surface charging which can significantly hamper both spatial and mass resolution as well as sensitivity. For insulating samples these are often prepared as thin sections ($\sim$1–20 μm) and mounted onto conductive substrates such as silicon, steel or indium-tin oxide coated (ITO) slides. It should be noted that charge compensation can enable analysis of insulating samples by actively neutralizing surface charge and such capabilities are available on commercial systems.

The primary advantage of SIMS over other MSI techniques is the ability to restrict the analyzed area down to $\sim$100 nm, with features resolved by several beam diameters, providing by far the highest spatial resolution of any MSI approach. As many (bio)materials applications require sub-micron spatial resolutions, SIMS has a distinct advantage over other approaches described below. Combined with the energetic desorption/ionization process, SIMS is particularly well-suited for analysis of inorganic materials and materials bound to surfaces *via* chemical bonds. However, compared to softer desorption/ionization techniques like MALDI and DESI, SIMS imparts significantly

more internal energy to desorbed molecules, resulting in substantial molecular fragmentation. In some cases this feature can be highly advantageous, *e.g.*, for analysis of elements, covalently-bound surface materials, and for detection of chemical tags covalently bound to molecules of interest. The high sensitivity of SIMS for elemental imaging is in part due to operation in the so-called ''dynamic-SIMS'' mode. In dynamic SIMS high ion doses ($>10^{13}$ ions cm^{-2}) are used to produce ions from a large fraction of the entire surface. Due to the high ion doses detection of only small molecular fragments and elements originating from the surface is possible due to accumulation of surface damage. The high spatial resolution and sensitivity offered by dynamic SIMS has recently been exploited in a unique approach termed nano-SIMS. In this approach a cesium or oxygen primary ion beam is used which can be focused down to $\sim$50 nm.[23] The unique MS design allows up to seven *m*/*z* channels to be continuously monitored whereby *m*/*z* information is obtained *via* angular separation in a magnetic sector analyzer. Detectable ions are either elements or diatomic fragments such as CH^-.[23–26] Examples of materials chemistry applications include the analysis of ^{13}C-enriched Resveratrol coated Fe_3O_4 coated nanoparticles whereby Resveratrol was detected *via* the enriched ^{13}C signal in areas where it was localized[27] and the simultaneous localization of isotope-labelled lipids and selected proteins through the use of fluorinated gold immunolabels.[28] Nano-SIMS has also been widely used to study dynamic chemical changes in biological systems by virtue of its high sensitivity and precise measurements of ion abundance.[29,30] For instance, *via* incorporation and monitoring of stable isotope enrichments (in these cases ^{15}N enriched thymidine), it has been possible to pinpoint stem cell generation in mice hippocampi[31] and relatively quantify the different origins of new cardiomyocytes.[32] Similarly, laser ablation inductively coupled plasma (LA-ICP) mass spectrometry provides a highly complementary approach to element imaging with SIMS. Several authors report the use of LA-ICP-MS to study the biological uptake of nanoparticles[33,34] and the *in vivo* degradation of metallic implants.[35–37] Although LA-ICP-MS cannot compete with the spatial resolution offered by SIMS, it offers excellent quantitative abilities enabling absolute surface concentrations of elements to be determined with high precision (typically 5–15% RSD).[38–40]

For applications that require information on molecular distributions, such as untargeted (bio)molecular investigations, softer interrogation of the surface is needed. In these cases, a technique known as ''static SIMS'' can be utilized. In static SIMS, the ion dose is maintained below 10^{13} ions per cm^2 (the ''static-limit'') ensuring less than 1% of the surface is impacted by a primary ion. Thus, surface damage is minimized and the probability of detecting larger *m*/*z* species having *m*/*z* values up to $\sim$2000 is greatly enhanced. Although detection of intact labile molecules with molecular weights above 500 Da can still be a challenge, characteristic molecular fragments are often detectable under such conditions using traditional ion beams. For example, lipid analyses mostly result in the detection of lipid fragment ions (*i.e.*, the phosphatidylcholine headgroup ion at *m*/*z* 184 in positive-ion mode or free fatty acids in negative-ion mode) rather than the intact lipid itself, complicating interpretation of results.[11,25,41]

Driven by the increasing need to detect larger molecules, primarily for biomolecular analysis, recent SIMS developments have heavily focused on the development of softer ionization sources that greatly minimize fragmentation and surface damage.[42] In particular larger, polyatomic sources such as C_{60}^+,[43–47] SF_5^+,[48–50] Au_n^+,[46,51–53] gas cluster beams such as Ar_n^+[54–56] and $[CO_2]_n^+$[57] and recently water cluster beams[58] have revolutionized SIMS and brought it into the realm of true molecular analysis. With these sources it is possible to generate intact molecular information at ion doses above the static limit due to the drastically reduced surface damage of these large primary ions.[44] In these cluster ion sources a single primary ion can have a mass of up to 100 000 Da which greatly reduces fragmentation and subsurface damage, thereby enabling both softer ionization and sputtering (see below).[59] It must be noted that large cluster beams do not generally offer the $\leq$100 nm[42] spatial resolution of atomic or small cluster sources (*e.g.*, Bi_3^+). The current state-of-the-art of cluster sources can achieve focused spot sizes down to several micrometers for gas cluster ion beams and in some cases as low as 300 nm for C_{60}^+ ion beams.[60,61] It should be noted that despite the tremendous advances made in molecular detection with SIMS over recent years many applications still center on the detection of elements or elemental/small molecular markers of larger molecules.

A second key advantage of SIMS over other MSI techniques is the exploitation of the gradual removal of material by the primary ion beam to enable 3D analysis (*i.e.*, depth profiling).[62,63] In such an approach a cluster ion beam is often used to sputter away several monolayers or more of material while minimizing surface damage and modification, after which the freshly exposed surface is imaged using SIMS. This process can be repeated using sequential sputter/analysis cycles and enable 3D chemical reconstruction of heterogeneous materials. Crucially, the achievable depth resolution can be as low as several nanometres,[64,65] providing almost a monolayer by monolayer representation of the material. In the sections below, we highlight a diverse array of applications of SIMS-MSI in materials chemistry with specific emphasis on biomaterials and their interactions. For a more comprehensive examination of biological tissue imaging applications of SIMS-MSI the reader is referred to a series of reviews published on this topic.[25,41,66–75]

Synthetic polymers

SIMS-MSI has found widespread use for studying polymeric materials in a diverse array of applications.[76–78] For example, using a 5 keV Ar_{2000}^+ beam for sputtering and a Bi_3^+ beam for mass analysis, the composition of spin-cast polymer multilayers contacting alternating layers of polystyrene (PS) and polyvinylpyrrolidone (PVP) on silicon substrates has been studied.[79] Polymer signals were identified by the characteristic $C_7H_7^+$ and $C_6H_{10}NO^+$ signals for PS and PVP, respectively and incorporated PS layers as thin as 45 nm could be resolved. A similar approach has also been employed using C_{60}^+ for sputtering instead.[80] 3D-SIMS has also provided valuable insight into surface

topographies of poly(bisphenol A-*co*-decane ether) films. SIMS, for the first time, revealed the presence of hollow interior structures on the surface of these polymers when prepared with either chloroform or THF solvents. These hollow droplets were found to have a thickness of several hundred nanometers and were sandwiched between the two polymer layers.[81] As another example it was recently shown how polyelectrolyte multilayer composite films could be synthesized and exposed to a mineralization process. The quality of polymeric nucleating agents was assessed in terms of calcium carbonate mineral infiltration efficiency by SIMS depth profiling with a combination of a Bi^+ beam for analysis and a cluster Ar_n^+ beam for sputtering.[82] With respect to biomaterials Jung *et al.* have deployed 3D-SIMS to study the spatial distributions of the biopolymers cellulose and lignin in tension wood as a model for biomass using a Bi_3^+ beam for analysis and an O_2^+ beam for sputtering.[83] Finally, in a recent publication by Goor *et al.*, the reactions of incorporated materials within a supramolecular assembly were studied with 3D-SIMS-MSI (Fig. 1).[84] An ureidopyrimidinone (UPy)-based matrix serving as a thermoplastic elastomer was mixed with reactive UPy-tetrazine (UPy-Tz) additive. The UPy-Tz provides supramolecular intercalation into the UPy to generate a functionalized surface. To assess which UPy-Tz concentration resulted in the most surface-localized functionalization an area of 100 × 100 μm was imaged with a Bi_3^+ beam following each C_{60}^+ sputter cycle. At low UPy-Tz concentrations the fluorine signal (specific signal to UPy-Tz model compound) was localized at the surface of the material. At higher concentrations UPy-Tz-related signal was also observed throughout the bulk material, but with higher intensity always on the surface. Proof of successful click-reaction was provided by the surface-exclusive detection of iodine following the click-reaction of *trans*-cyclooctene iodine with intercalated UPy-Tz. Combined with the homogenous distributions throughout the film of UPy and monomers of the polycaprolactone (PCL, also part of the elastomer), localized chemical analysis in 3-dimensions using SIMS was able to directly visualize differences in surface and bulk reactivity as relevant for functionalization of supramolecular materials.[84] The authors conclude that such materials and functionalization reactions may find use in regenerative medicine where *in vivo* functionalization may be exploited to elicit the required materials–tissue/cell interactions.

Nanoparticles

The ability to track nanoparticles within cells is attracting much interest in the analytical field due in part to the development of nanoparticles capable of delivering therapeutics intracellularly.[85–90] SIMS has proven a useful tool for studying such materials and their interactions.[10,87,89,91–96] In a recent study, Hua *et al.* described an innovative microfluidic/sputtering approach allowing SIMS imaging of individual cells in a hydrated environment.[97] This was used to study the effect of ZnO nanoparticle uptake in C10 cells with sub-micron resolution. Nanoparticle uptake was visualized by the characteristic Zn^+ signal while nanoparticle containing cells were observed to exhibit elevated Ca^+ and decreased Na^+ and K^+ signals that were attributed to altered intracellular Na^+ and K^+ transport induced by ZnO nanoparticle uptake.

By using a C_{60}^+ source for both sputtering and analysis both organic and inorganic materials can be imaged in 3D in a single experiment. This was shown by Angerer *et al.* for the 3D MSI of a titanium dioxide nanoparticle engulfed by a unicellular eukaryote,

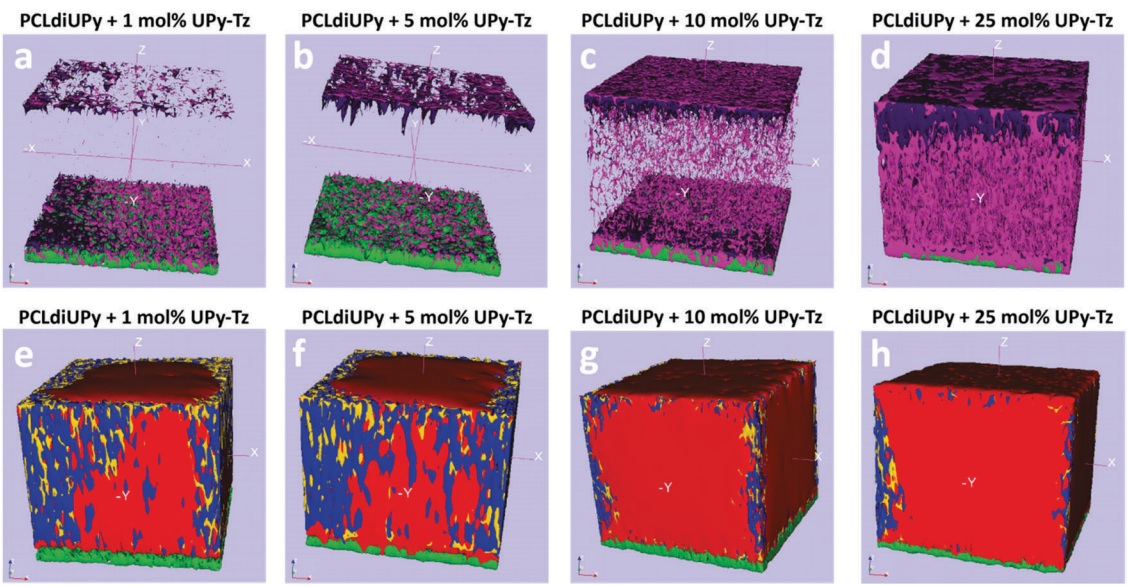

Fig. 1 A 3D-reconstruction of increasing concentrations of mixed-in guest molecules (Upy-Tz) within a UPy thin film using SIMS-MSI where click-chemistry to an iodine containing model compound was performed on the surface. The ion distributions of relevant mass fragments are depicted in different colors: iodine (purple, TCO fragment), fluorine (pink, from Upy-Tz), *m*/*z* 124 (red, UPy-fragment), *m*/*z* 150 (blue, UPy-fragment), *m*/*z* 113 (yellow, PCL-fragment), InO_2 (green, from glass slide substrate). The films have a thickness of 100–150 nm. Dimensions of depth profile area are 100 μm × 100 μm. Figure reproduced and adapted from ref. 84 with permission from John Wiley & Sons.

Tetrahymena pyriformis, where visualization of the incorporation of nanoparticles inside food vacuoles of the eukaryote was observed.[88] Another powerful example of 3D ToF-SIMS on polymer nanoparticles is given by Rafati *et al.*[98] The surface heterogeneity and relative localization of the poly(lactic-*co*-glycolic) acid (PLGA) backbone, polyvinyl acrylate (PVA) surfactant, and protein lysosome (model therapeutic) were visualized to gain understanding in the effect of polymer microsphere fabrication parameters and revealed that the lysosome was primarily distributed around microsphere surface pores.

Multimodal approaches with SIMS, such as with fluorescence or transmission electron microscopy (TEM), have proven especially useful to track nanoparticles in biological matrices.[28,99] Several studies have reported cytotoxicity assessment of nanoparticles with ToF-SIMS, such as Fe_3O_4 nanoparticles[100] or polymeric nanoparticles combined with fluorescence microscopy.[101] Recently, the delivery of cytotoxic drugs was evaluated by polymeric oxaliplatin nanoparticles through monitoring of the time-dependent spread of both the nanoparticle carrier and the Pt(II)-based anticancer drug *in vivo*. The combined fluorescence microscopy, TEM and SIMS approach discovered the oxaliplatin NPs are taken up in intracellular vesicles. The consecutive breakdown of the carrier material stimulates release of the cytotoxic drug, confirming the targeted delivery mechanism.[102]

Tissue engineering/cell culture

Tissue engineering is a young, thriving field of study clearly in need of imaging techniques with the ability to differentiate biological responses based on changes in local molecular composition. For example, SIMS has been deployed to study the homogeneity of cell populations based on their molecular phenotype[103] and shed light on the biological pathway changes related to culturing conditions.[104] SIMS can also be applied to evaluate the potential of tissue engineering stem cell lines. For instance, the osteogenic differentiation capabilities of human embryonic stem cell-derived mesodermal progenitors (hES-MPs) were studied and compared to human mesenchymal stem cells (hMSCs), one of the most documented cell types for tissue engineering purposes.[105] Using 3D-SIMS-MSI depth-profiling and 3D-mapping, distinct biomineralization patterns were shown, with hES-MPs yielding higher hydroxyapatite signal than hMSCs after six weeks but lower after 3 weeks of osteogenic stimulation.[106]

As ToF-SIMS offers exciting opportunities to correlate surface chemistry to biological response it is well suited to guide substrate development for proliferation and differentiation control.[107–109] Such an approach has been utilized to assess the cell proliferation effect of hydrogel substrate additives,[110,111] naturally derived extracellular matrices,[112–114] and surface geometries.[115] Current state-of-the-art substrates tend to have complex compositions and geometries, which require more specific and sensitive methods to verify. Bongo *et al.* showed their PEDOT(TOS):gelatin composite films were able to support cell growth while retaining the beneficial electrical conductivity and mechanical properties of the original polymer substrate.[116] The authors used a nano-SIMS instrument to reveal the distribution of carbon, nitrogen and sulphur and demonstrate the homogeneous gelatin incorporation in the film.

Implants

Successful implant integration in the surrounding tissue is of vital importance to patient health, but much remains unknown about the mechanics of implant–tissue interaction. In an effort to shed light onto these effects the interaction area between bone and a titanium implant has been imaged with ToF-SIMS, revealing distinctive molecular and elemental species for bone, implant, and interaction area.[117,118] Gonzalez *et al.* studied a bioactive coated Ti-NB-Hf alloy implant material using Bi_3^+ beam and showed this material had a significantly increased osteoblast adhesion.[119] In another study, the distribution of rapamycin – an immunosuppressant in a coronary stent coating (poly(lactic-*co*-glycolic acid)) – was studied to determine the effect of the coating application method on drug elution behaviour.[120] 3D-SIMS-MSI analysis showed a high degree of heterogeneity in the rapamycin concentration throughout the sample, with the most homogeneous areas providing the most gradual elution. It was therefore concluded that the coating application method has a major effect on the early drug elution behavior and therefore deserves thorough optimization.

Supramolecular materials such as biodegradable hydrogels are considered promising drug delivery carrier candidates. Ureidopyrimidinone (UPy) cross-linked poly(ethylene glycol): polycaprolactone (PEG:PCL) hydrogels implanted under the renal capsule of rats have been studied with Au^+ SIMS, comparing relative distributions of endogenous compounds (lipids and cholesterol) and the implanted polymer (PEG). Interestingly, it was observed that the PEG-related signal was co-localized in the tissue with cholesterol sulfate, suggesting the occurrence of cellular infiltration in the polymer.[121] This study demonstrates the vast potential of SIMS to study foreign-body response mechanisms and can help monitor material–tissue interactions, for example in drug-delivery applications.

Advances for chemical identification using SIMS

The use of axial ToF analyzers for SIMS requires the primary ion beam to be pulsed on the order of several nanoseconds to obtain reasonable mass resolution. However, this introduces both speed and sensitivity constraints due to the limited duty cycle resulting from the fact that only one ion packet may be injected into the analyzer per ToF event. For example, a 2 ns pulsed beam operating at 10 kHz and a maximum flight time of 100 μs means only 0.002% percent of the time is spent generating ions. To overcome these limitations and enable continuous ion generation several groups have developed SIMS instrumentation employing orthogonal ToF analysers.[122–124] Through decoupling of the mass analysis and ion generation these systems can take particular advantage of cluster ion beams. Their ability to generate intact molecular ions at higher ion doses with reduced surface damage makes them ideal to operate in continuous (DC) mode. That is, the beam is effectively generating ions 100% of the time resulting in significantly increased experimental throughput.[69] It should be noted that orthogonal ToF analyzers have less efficient transmission than axial ToF analyzers, sacrificing part of the theoretical gain in sensitivity and time.

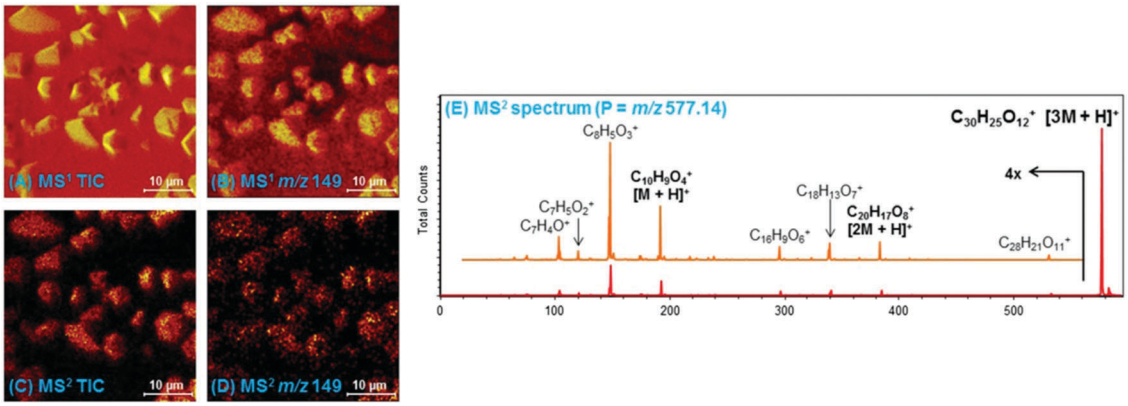

Fig. 2 Parallel SIMS-MS and tandem SIMS-MS/MS imaging of heat treated polyethylene terephthalate crystals. (A) Total-ion current (sum of all signals) image in full-MS mode. (B) Distribution of *m/z* 149 in full-MS (MS^1) mode. (C) Total-ion current (sum of all signals) image in MS/MS mode following selection and collision-induced dissociation (CID) of *m/z* 577 corresponding to the ethylene terephthalate trimer ion. (D) Distribution of *m/z* 149 in MS/MS mode revealing significantly less background and higher contrast images of the polymer crystals. (E) Corresponding MS/MS spectrum revealing structure-specific fragments arising from the polyethylene terephthalate ion after (CID). Figure adapted from ref. 128 with permission from Cambridge University Press.

Recent advances in SIMS have also enabled confident structural identification of detected molecules using tandem mass spectrometry (MS/MS).[122,124,125] Although such capabilities have long been available for MALDI and ESI-based instruments they were lacking for SIMS. Such approaches are critical for identifying unknown surface modifications and unresolved isobaric ions. To date, MS/MS technologies have been employed mostly for biomolecular characterization from tissues and cells.[122,126] However, structural elucidation/confirmation of detected molecules is also of high importance for materials characterization. A drawback of conventional tandem MSI approaches is the majority of generated ions are discarded, with only the fragments of the selected precursor detected. To overcome this disadvantage a parallel ToF tandem MS system based on an axial ToF design was recently developed.[125,127] The addition of a collision cell and second ToF analyzer to this design enables simultaneous recording of both MS and MS/MS spectra, thus providing both fragment ion (MS/MS) detection of a selected monoisotopic *m/z* range and broadband (MS) detection of the remaining ions. The increased chemical specificity enabled by MS/MS imaging was demonstrated for heat treated polyethylene terephthalate (PET).[128] Fig. 2 shows the total ion and *m/z* 149 images of which the latter is a known SIMS fragment of PET. The *m/z* 149 image, along with other images of ions in the full-MS spectrum, reveal the presence of polymer crystals, but these *m/z* signals also arise from the surrounding substrate resulting in ionic signal observed across the full sampling area. However, when imaging in MS/MS mode using the ethylene terephthalate trimer ion (*m/z* 577) as the precursor, the same PET-characteristic fragments are also produced upon collision-induced dissociation. Importantly, these are now detected in the absence of isobaric interferences as the MS/MS detector is only detecting the *m/z* 149 signal that originates from the polymer-related precursor. With the use of tandem MS imaging the background interference is eliminated and the polymer crystals are observed with higher contrast at a measured lateral resolution of <200 nm while the composition of the crystals was unequivocally found to be ethylene terephthalate trimers.

With the increased ion yields for larger molecules when using cluster sources the intrinsically moderate mass resolution of a ToF analyzer begins to become a limitation. It is widely known that in the analysis of complex mixtures, multiple ions are produced with the same nominal mass but different elemental composition and thus exact mass. Although high resolving power instrumentation is widely available and compatible with MALDI and various ambient ionization methods, this has not been the case for SIMS. In an effort to resolve the molecular complexity of biological surfaces using SIMS Smith *et al.* have orthogonally coupled a C_{60}-SIMS source with a Fourier transform ion cyclotron resonance mass spectrometer (FT-ICR MS).[129] FT-ICR provides at least an order of magnitude increase in mass resolving power compared to ToF systems and is able to provide more specific chemical information from a complex sample. For example, by applying SIMS-FTICR-MSI to the analysis of a mouse brain nine different chemical features were detected within a 0.4 Da mass range. The high mass accuracy also allows elemental formula for many detected species to be rapidly assigned.[130] The main drawback of this approach, however, is the sacrifice in required speed and/or spatial resolution resulting from the longer dwell times needed per pixel to accumulate enough ions for adequate signal-to-noise ($\sim$0.4 s per pixel). With current developments in the coupling of SIMS with FT-based mass spectrometers, such as the 3D nanoSIMS project,[131] it is expected that such approaches will soon find powerful usage for analysis of localized chemical composition in the materials sciences.

Matrix-assisted laser desorption/ionization (MALDI) and direct laser desorption/ionization

The discovery of matrix-assisted laser desorption/ionization (MALDI) in the late 1980s was pivotal in the birth of macromolecular MSI (*i.e.*, intact molecular detection).[132–134] For the first time,

MALDI enabled the direct detection of many different molecular classes from solid substrates, including large fragile biomolecules such as intact proteins, with minimal fragmentation. MALDI is used almost exclusively for organic molecules, however analysis of inorganic materials is also possible,[135,136] while direct laser desorption (*i.e.*, without the matrix) can also be employed for inorganic materials.[137] In MALDI, the sample is first mixed with an organic matrix having strong absorption at the typical wavelength used for desorption (337 or 335 nm). After mixing, the analyte molecules are co-crystallized with the matrix to form co-crystals. Typically, the sample is then loaded into a vacuum stage varying anywhere from 1 mbar to 1×10^{-7} mbar for analysis depending on the instrument design. In efforts to simplify sample analysis MALDI analysis at atmospheric pressure is also possible[138,139] but less commonly used, in part due to the lower sensitivity resulting from the difficulties in transferring ions from atmospheric pressure into the intermediate vacuum region of the mass spectrometer. MALDI typically requires flat (roughness in low micrometer scale), thin (typically 4–20 μm) samples to ensure equal irradiation conditions across the sample and to help minimize charge build up. Surface charging is only a major issue for axial-ToF analyzer (the most widespread analyzer for MSI) and its negative effect is ameliorated by mounting the sample on a conductive substrate (*e.g.*, ITO coated glass slides) onto which the high ion acceleration voltage is applied. Orthogonal mass analyzers (*i.e.*, those with ionization and mass analysis regions decoupled) can accept insulating substrates without reducing MS performance. Upon irradiation by a pulsed UV laser, desorption is initiated with the majority of the energy being absorbed by matrix molecules. Analyte ionization occurs through a series of gas-phase reactions initiated by photoionised matrix molecules and ultimately charge transfer to the analyte with protonated/deprotonated or alkali-adducted (*i.e.*, $[M + Na]^+$) ions generally observed. Unlike SIMS, MALDI is not strictly a surface analysis technique due to the matrix solution extracting molecules from within a volume of the sample surface and its relatively large sampling depth (~several micrometers per sampling position when multiple laser shots are accumulated). When corrected for sampling volume, it has been reported that under favorable conditions SIMS can be up to several orders of magnitude more sensitive than MALDI.[140,141] However, unlike SIMS, the MALDI process is soft and minimal fragmentation is observed resulting in significantly more interpretable chemical information from complex surfaces.

As MALDI enables localized analyses, the extension to imaging was first taken in the mid-90s[142] and has since been the key driver in the development of MSI, particularly for biomolecular imaging in tissues.[70,143–145] MALDI is currently the most common method for MSI due to its high sensitivity, significant commercial development, and ability to detect the most diverse array of molecular classes of any MSI technique. For imaging applications, the MALDI matrix is typically applied using either a pneumatically-assisted spray, sublimation, or controlled droplet deposition (*i.e.*, piezoelectric printing). For all applications it is essential to ensure a homogenous coverage of matrix with minimal analyte delocalization on the surface. The application of the matrix presents the greatest source of error in the reproducibility of MALDI measurements. MALDI spatial resolution is determined by the size of the matrix crystals and the laser beam diameter on the surface and is currently at-best 5–10 μm in commercial instruments and as low as 1 μm in prototype systems.[146–148] It should be noted resolutions $\leq$10 μm typically requires matrix application *via* sublimation which can compromise analyte extraction, and thus sensitivity, relative to spray-based approaches. To-date almost all MALDI-MSI applications have focused on biological tissue imaging and for these the reader is referred to relevant reviews.[70,143,144,149] The extension of MALDI-MSI to materials chemistry applications remains, in our view, a dramatically underexploited field. Below we outline recent examples where MALDI-MSI has provided valuable insight into the localized chemical changes occurring during the processing and preparation of various materials.

MALDI has found widespread use for the chemical analysis of polymeric substrates.[118,119] These capabilities have recently begun to be extended to visualizing localized chemical changes occurring on polymeric materials designed for a variety of applications. For example, Crecelius *et al.* have applied MALDI-MSI to visualize chemical changes within polystyrene (PS) films exposed to ultraviolet (254 nm) light.[150] Polymer films were prepared by mixing PS solutions (PS, $M_{n,SEC}$ = 4760 g mol^{-1}, $M_{w,SEC}$ = 5000 g mol^{-1}) with toluene, matrix (*trans*-2-[3-(4-*tert*-butylphenyl)-2-methyl-2-propenylidene]malononitrile) and AgTFA dissolved in THF and spin coating this mixture onto indium-tin-oxide coated (ITO) slides. Shaped masks were then placed onto the films prior to UV irradiation for different times. Comparison of areas exposed to UV light revealed the gradual loss of polymer signals with exposure time which were attributed to polymer cross-linking upon photo-generation of backbone radicals. The ability to monitor surface modification upon light irradiation opens up the possibility of studying the chemical changes occurring on photoresists and performance coatings.[151] Here a negative photoresist (Novolac) containing benzophenone photo-activator (10% w/w) was used and a wiring diagram imprinted onto the surface with UV light. The substrate was imaged with a resolution of 100 μm, and polymer signals characteristic of the Novolac resin monitored. Of significance was a decrease of the undodecamer and tridecamer polymer signals in areas exposed to UV light. This loss in signal correlated with areas of lithographic imprinting and again was attributed to photo-induced polymer crosslinking, thus demonstrating the capability of MSI to study the chemical changes induced by lithographic structuring such as that used in PCB board manufacture.

Polymer MSI has also been applied to study heterogeneous biotic and abiotic degradation of polycaprolactone diol in water.[152] After incubation in biotic (artificial stream) and denitrifying (liquor from a waste water treatment facility) solutions the polymer materials were sectioned and studied with MALDI-MSI. Whereas the chemical composition following aerobic (biotic) conditions was only slightly altered, the sample exposed to denitrifying conditions revealed evidence for significant polymer degradation

(loss of signal intensity) and oxidation. Degradation was observed to occur more heterogeneously throughout the polymer material when exposed to denitrifying conditions, thus further demonstrating the power of MSI to study localized degradation processes of polymers and other substrates.

Ultrahigh molecular weight polyethylene (PE-UHMW) is a widely used material for replacing the acetabular cup of hip and knee joints. Despite this popularity, it suffers from relatively short lifetime with replacement often needed every 5–10 years.[153,154] Oxidation of the polymeric material has been recognized as a major contributor to this short life time. An interaction of the PE-UHMW with the surrounding biological environment consisting of synovial fluid is an important contributor to polymer modification. In this light, Fröhlich *et al.* have recently applied MALDI-MSI to study adsorption of lipids from the synovial fluid onto the polymer surface and its correlation with surface modification.[155] Following incubation of PE-UHMW in synovial fluid, the polymeric material was analyzed with both MSI (spatial resolution of 10–150 μm) and SEM. After incubation, polymer surfaces were roughened and adsorption of biological materials could be observed with SEM. MSI allowed the localization and structural identification of adsorbed lipids such as PC, PE and cholesterol directly from the substrates. Chemical specificity of MSI was increased by performing MS/MS imaging whereby characteristic fragment masses are detected and visualized. Localization of lipids was found to correlate with the presence of roughened substrate features. Given the strength of MSI to detect many molecular species simultaneously, detection of the polymer substrate itself was also possible. Interestingly, oxidized PE-UHMW was detected by *m*/*z* spacing of 74 indicative of PE-UHMW hydroperoxide, and was also found to be localized in areas of high lipid adsorption. Combined, application of MALDI-MSI to joint replacement materials provided the first evidence of preferential adsorption of lipids from synovial fluid onto roughened and oxidized surface areas. Oxidation can be rationalized by presence of reactive oxygen species in synovial fluid which can have detrimental effects on implant lifetime. Given the lubricating nature lipids play in both native and artificial joints, MSI provides a promising tool to help develop new joint materials that promote positive interactions with the surrounding biological environment. The same authors have also reported on the use of MALDI-MSI for localization of proteins adsorbed onto PE-UHMW incubated with synovial fluid.[155] On flat samples homogenous protein distributions were observed, while preferential adoption onto roughed or folded areas was observed. In line with the lipid results, this suggests that *in vivo* damaged regions are more susceptible to protein adsorption which may alter implant properties. In related applications concerning the localized interactions of biomolecules with biodegradable materials MALDI-MSI has also been deployed to study lipid and protein adsorption onto thermoplastic polyurethane grafts for vascular replacements.[156,157] For example, in one study by Fröhlich *et al.* the diffusion of cholesterol into the synthetic vessels wall was observed and tentatively attributed to the favorable thermoplastic polyurethane pore size facilitating small molecule diffusion.[157]

Insight into the self-assembly behavior of mixed peptide fibers has also been recently obtained with MALDI-MSI.[158] Self-assembling peptides (peptide 1 = IKHLSVN, peptide 2 = IKFLSVN and peptide 3 = IKYLSVN) were mixed into various two component systems and deposited onto ITO slides where they aged over time. After matrix application peptide fiber distributions were imaged using high resolution FTICR-MSI. Mixture A (peptide 1, Fig. 3, cyan) and peptide 2 (Fig. 3, magenta) was found to initially form long fibers with a relatively homogenous distribution of the two peptides (days 1–2). This state was hypothesized to be only kinetically stable. During days 3–4 the fibrils became smaller and this was correlated with fiber rearrangement

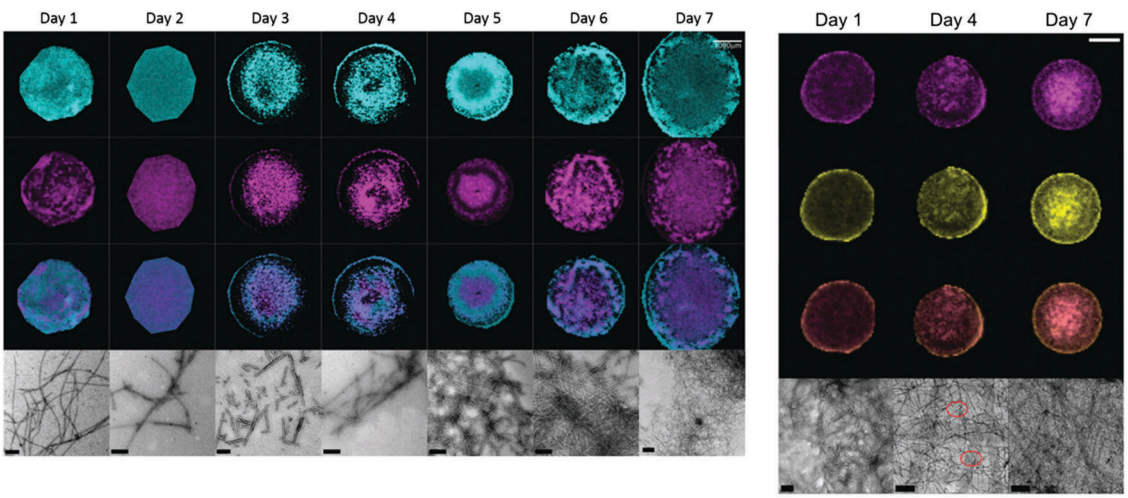

Fig. 3 (left) Time-series MALDI-MSI images of a two component peptide mixture (IKHLSVN in cyan and IKFLSVN in magenta) from day 1–7. An overlay of these two images is provided in the third row. (right) Time-series MALDI-MSI images of a two component peptide mixture (IKFLSVN in magenta and IKYLSVN in yellow) after 1, 4 and 7 days. An overlay of these two images is provided in the third row. Both MALDI-MSI datasets show the self-assembly process of the fiber mixtures. TEM images of the corresponding mixtures are provided below the respective MSI images. Reproduced from ref. 158 with permission from The Royal Society of Chemistry.

and segregation of the individual peptides. This process was observed until day 7 upon which a thermodynamic steady state is reached and only segregated, individual fibers are observed. In contrast, peptide mixture 2 (peptide 2 and 3) initially formed a thermodynamically stable system whose morphology did not change significantly over time. MALDI-MSI revealed that both peptides were homogeneously distributed. TEM analysis revealed intermixed flat ribbon and twisted structures which were assumed to each correspond to single component fiber. Differences between the mixtures were attributed to the different hydrophobicity and non-covalent interactions. Unlike optical imaging techniques that require labelling which can interfere with the self-assembly process, direct MSI analysis permits analysis of the unmodified peptides and study of their self-assembly behavior into organized kinetically and thermodynamically favored structures.

Carbon nanomaterials are attracting much interest for a diverse array of applications, including biomedical applications where they are loaded into the body. In such applications it is critical to understand how they are metabolized and in what organs they accumulate. Recently, laser desorption/ionization (LDI) has been applied to directly visualize the sub-organ accumulations of carbon nanotubes (CNTs), single-layer graphene (GO) and carbon nanodots (CD) after injection into mice.[159] In this approach direct LDI of dosed tissues (*i.e.*, without the application of a MALDI matrix) was used to directly detect carbon nanomaterial by virtue of their low mass carbon cluster signals (*e.g.*, C_n^-, n = 1, 2, 3, 4, 5, *etc.*). Carbon nanomaterials could be rapidly detected in various tissues such as kidney, spleen, lung, liver, brain and heart tissue. For example, Fig. 4 shows results obtained from mice spleen revealing preferential accumulation of CNTs in the marginal zone of the spleen with subsequent lower concentrations observed in the red and white pulp, respectively. Quantitative MSI using dosed tissue homogenates for signal calibration was also performed and after calibration the maximum signal could be calculated to be ~8 pg/20 μm pixel for CNTs in the spleen. Calculated detection limits were 0.02, 0.04 and 0.10 μg ml^{-1} for CNTs, GO and CDs, respectively. Quantitative results revealed the largest uptake of CNTs and GOs in the lung, while CDs preferentially accumulated in the spleen. The extension of this method demonstrated the selective accumulation of drug-loaded CNTs into a tumor, thus providing a powerful tool for targeted drug delivery applications. In another application LDI-imaging of inkjet-printed patterns of functionalized gold nanoparticles has also been demonstrated.[160]

The above examples highlight a diverse array of materials-chemistry-focused MALDI-MSI applications. However, when compared to applications to biological tissues, these relative numbers are quite low. Nonetheless, we believe that the unique ability of MALDI-MSI to detect most molecular classes, combined with the extensive ability of high performance commercial instruments offering both high spatial resolution (10 μm) and high mass resolution, should make it a powerful approach for many researchers and industries where understanding the localized chemical composition, its changes to external factors, and interaction with the surrounding environment is key for material design and performance. It can be expected such approaches will increase in popularity in the near future.

Emerging MSI methods with potential for biomaterial applications

Over recent years much work in the MSI field has focused on making a broader range of samples accessible. An important

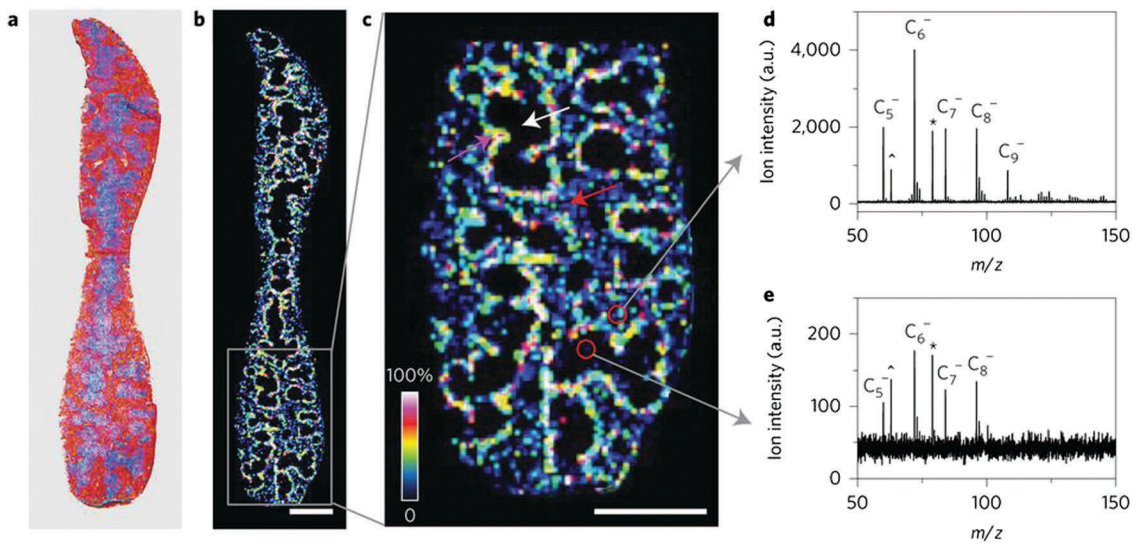

Fig. 4 Mapping of sub-organ distributions carbon nanotubes (CNTs) in mice spleen using direct laser desorption/ionization (LDI). (a) Optical image of the spleen tissue. (b) Ion distribution of CNT-specific m/z 72.0 throughout the spleen. (c) Expanded region of (b) revealing accumulation of CNTs in the red pulp of the spleen. Representative LDI mass spectra acquired from red and white pulp regions (d and e, respectively). Scale bars are 2 mm. Reproduced from ref. 159 with permission from Springer Nature.

requirement for the methods discussed above is the requirement that the samples be placed in vacuum. As a result, many samples (such as those containing water) cannot be analyzed in conditions that closely mimic their natural state. These requirements have spawned the field of ambient MSI methods that, despite generally offering lower spatial resolution (typically ~50–300 μm), enables MSI analysis of samples in the open environment without any sample pre-treatment (*e.g.*, matrix application). The following section will briefly discuss different MSI techniques that, although have very few reported applications to biomaterial analysis to-date, have the potential to be very useful, and possess some unique qualities that are not shared by SIMS or MALDI. These techniques may be complementary to SIMS and MALDI analyses or employed for certain applications where SIMS or MALDI are not applicable, such as non-vacuum compatible samples.[161–169] These ambient MSI techniques can be highly adaptable, allowing optimization for different sample shapes and sizes with minimal effort.

One of the most popular ambient MSI techniques is desorption electrospray ionization (DESI) due to its simplicity and relative ease of operation.[161] For DESI, charged solvent droplets impact the surface creating a very thin fluid layer where analyte extraction and subsequent desorption occurs.[161,170] The spatial resolution achievable with DESI imaging is generally ~150 μm, however with optimized hardware and experimental parameters resolutions as low as 35 μm have been reported.[171–173] DESI-MS imaging offers lower spatial resolution than MALDI or SIMS due to the spray based desorption/ionization but is particularly useful for samples that are bulky, irregularly shaped, or require enhanced extraction of analyte from the substrate.[174] DESI-MSI has been applied mostly to biological tissue analysis,[175] although various other substrates such as TLC plates, rocks containing heterogeneous mineral deposits, bulk polymers and polymer coatings, and organic materials have also been studied.[176,177] For example, in the analysis of thermoset polymer-based coatings the performance of formulated antioxidants could be measured *in situ* without any sample pretreatment (Fig. 5).[177] Another example showcasing the broad applicability of DESI-MS is the surface analysis of biocompatible polymers *ex vivo*, providing insight into their interactions with living tissue. Suder and co-workers employed DESI-MS to investigate the plaque deposits on a polyethylene terephthalate vascular graft that was removed from a patient after 2 years serving to replace part of the femoral artery.[178] Imaging cross sections of the plaque deposits revealed changing lipid profiles associated with atherosclerotic plaque formation and saturation of the polymer surface by endogenous lipids. These results demonstrate that DESI-MS is an ideal analytical approach for biomedical applications where artificial and biological materials interface due to its selectivity and relatively soft method for probing the sample.

Alternative solvent extraction-based techniques have been developed that differ from DESI by decoupling the extraction and ionization steps.[179–183] These techniques have yet to be exploited for any true biomaterials applications but have potential use in the field including; liquid microjunction solid sampling probes (LMJ-SSP) in their various forms, nano-DESI,

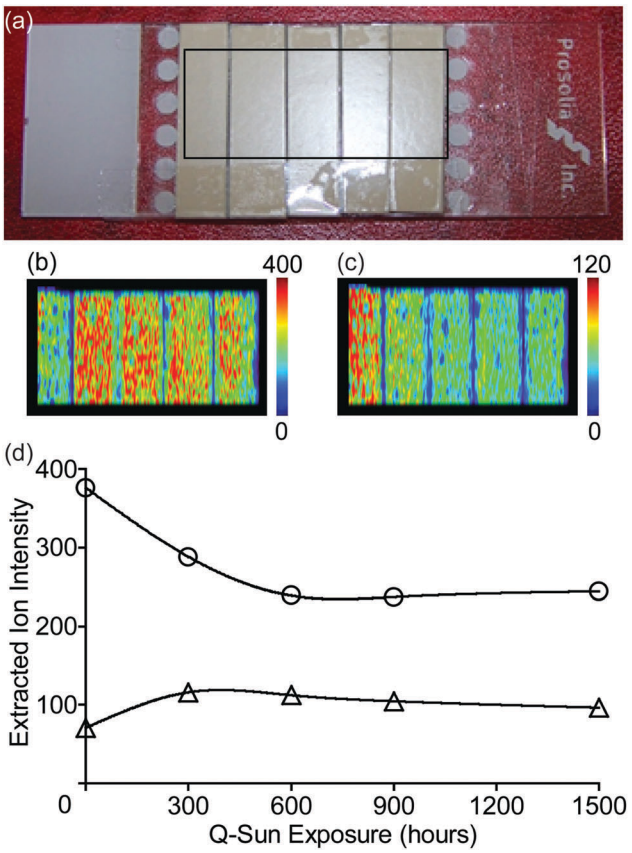

Fig. 5 (a) A photograph of a double draw-down panel consisting of two polyester-based paint formulations, a green pigmented coating containing no HALS (left) and a brown pigmented coating (right) containing TIN123 (2 wt% of resin solids). (b) A representative extracted ion chromatogram (XIC) of the *m/z* 737.5 ion corresponding to $[M + H]^+$ ion of TIN123 acquired across the panel left-to-right using DESI-MS. (c) A photograph of coil coated metal samples cut from panels that were exposed to 0 (far left), 300, 600, 900, and 1500 h (far right) of Q-Sun artificial weathering and affixed to a microscope slide, and the resulting false color images of the extracted ion intensities (ion counts) at (b) *m/z* 737.5 and (c) *m/z* 609.5 by 2D DESI-MSI. (d) Extracted ion chromatograms integrated over 50 mm^2 for each exposure interval (0, 300, 600, 900 and 1500 h) for the ions at *m/z* 737.5 (open circle, ○) and *m/z* 609.5 (open triangle, △). Reproduced and adapted from ref. 177 with permission from The Royal Society of Chemistry.

and liquid extraction surface analysis (LESA). The first two involve a continuous flow of solvent in contact with the surface, desorbing analytes at the point-of-contact followed by aspiration through an electrospray emitter. In comparison, LESA uses discrete amounts of solvent contained within a pipette tip to create a temporary liquid microjunction with the surface.[184–186] LESA is well equipped for applications where sample carryover interferes with continuous imaging experiments but does limit the spatial resolution to >0.5–1 mm.[187] These liquid microjunction techniques would be excellent candidates for the analysis of delicate gels and nanofabricated materials that are not amenable to lasers, heat, or pneumatically-assisted sprays. For example, hydrogel scaffolds containing cell cultures or organoid assemblies, or where the surface integrity needs to be highly maintained for further analyses after MSI. For example,

LESA-MS has been applied to study the deposition of tear lipids on worn contact lenses demonstrating the ability of such techniques to study the molecular processes associated with biofouling of polymeric surfaces.[188]

Laser desorption based techniques

Laser desorption/ablation based techniques are becoming increasingly popular for ambient MSI due to their high spatial resolution (down to 10 μm sampling spot size) and ability to be coupled to solvent sprays and plasma plumes for enhanced ionization. Three major techniques have been reported for MSI that combine laser ablation (LA) with an electrospray ionization source; laser ablation electrospray ionization (LAESI),[189] electrospray-assisted laser desorption ionization (ELDI),[190] and laser electrospray mass spectrometry (LEMS).[191] For these techniques the experimental setup is the same, differing only in the type of laser employed to ablate material that is then entrained within the electrospray plume flowing on-axis towards the MS inlet.[192,193]

Another technique with high potential for biomaterial applications is an LMJ-SSP coupled with transmission laser ablation, being employed for the detection of insoluble surface components such as small oligomers of polyaniline and elemental analyses from thin metallic films.[194] This ambient imaging technique represents an ideal method for surface analyses where changing distributions of soluble analytes correlate with insoluble, heterogeneous polymer or metal substrates as this technique, theoretically, could be able to characterize both sample and substrate in a single acquisition.

Thermal desorption based techniques

A recent innovation by Van Berkel and co-workers has led to the development of a thermal desorption (TD) imaging technique that provides the highest spatial resolution for ambient MSI currently reported.[195,196] The technique combines atomic force microscopy (AFM) with MS where a hybrid sampling probe provides co-registered topographical, band excitation nano-mechanical,[197] and chemical imaging of a surface.[198,199] By heating the AFM tip to 350 °C, thermal desorption coupled with ESI or atmospheric pressure chemical ionization (APCI) can be applied to surfaces with a spatial resolution corresponding to 2.0 μm × 2.5 μm pixel sizes.[198,199] The technique has been applied to printed inks, bacterial colonies on agar plates, and phase-separated polystyrene/poly(2-vinylpyridine) polymer blend thin films. For the polymeric samples, chemical compositions of valley and plateau regions within the surface were identified by co-registering topographical measurements and band excitation images with mass spectral chemical images (Fig. 6a–d).[200]

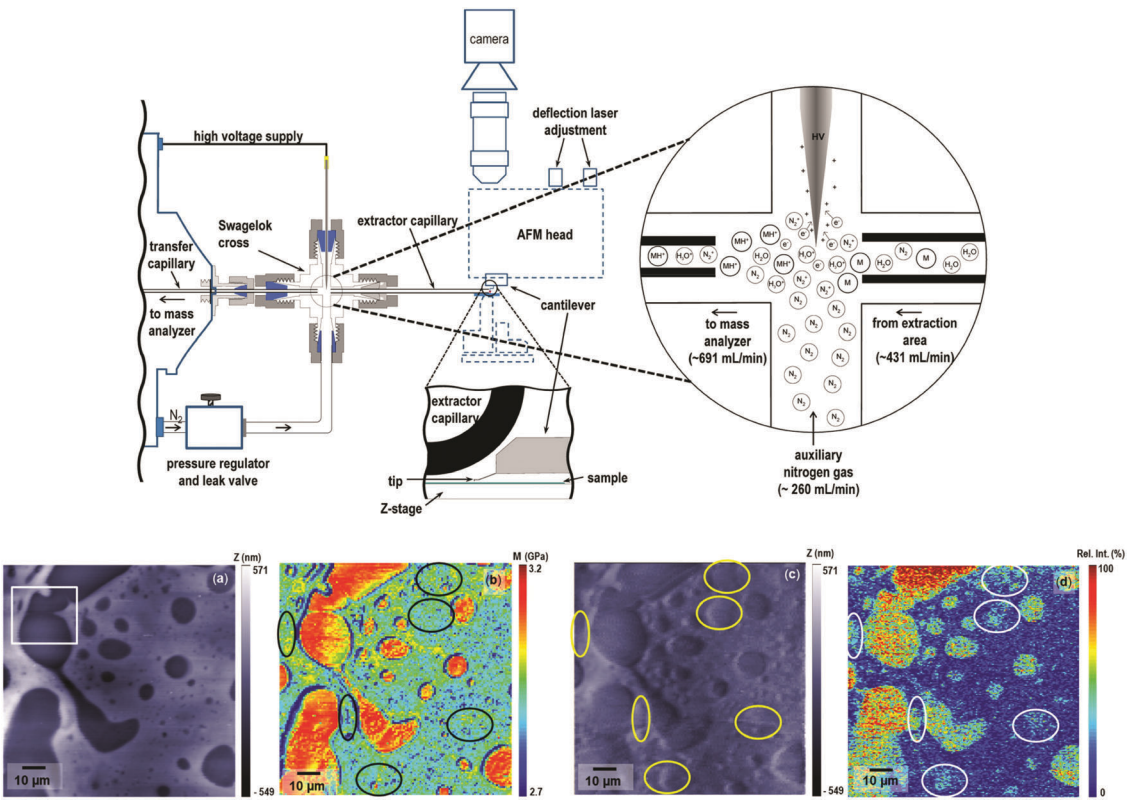

Fig. 6 A schematic illustration of the combined AFM-MS experimental setup with an enlarged view showing the details of the inline APCI and ion molecule chemistry and an enlarged view of the AFM nano-TA probe positioned ~0.3 mm away from the sampling capillary. Co-registered AFM (a) pre-pyrolysis topography image, (b) BE elastic modulus image, (c) post-pyrolysis topography image, and (d) mass spectrometry chemical image for m/z 106, obtained from an ~500 nm thin film of phase-separated polystyrene/poly(2-vinylpyridine) blend. The color scale for the topography goes from dark to light, which is proportional to an increase in relative surface height. Highlighted ovals in panels (b–d) indicate areas where the AFM topography, elastic modulus, and mass spectrometry images differ in terms of the presence of P2VP. Reproduced from ref. 200 with permission from American Chemical Society.

Fig. 6 also shows a schematic representation of the AFM-MS setup designed by Van Berkel and co-workers and is an excellent example of the relative ease that ambient MS affords for *ad hoc* instrumentation. The AFM-MS technique also demonstrates the capability of simultaneous multimodal imaging data acquisition, providing added layers of information to each voxel in the dataset through co-registration of multiple imaging modalities.

Conclusions

The growing use of MSI for (bio)materials chemistry analyses is evidenced by the number of excellent applications detailed in this review. However, there is scope for MSI to be an even greater resource in the field of biomaterials research. *Via* this review we have not set out to provide a comprehensive review of all reported applications of MSI in the materials sciences, but rather have endeavored to convey the unique opportunities alternative techniques offer to materials chemistry investigators. By highlighting the broad chemical sensitivity, specificity, and structural elucidation capabilities afforded by mass spectrometry and its complementarity with other surface imaging techniques we hope to illustrate the usefulness of MSI approaches available to the materials science community. The ability to analyze many different molecules in a single experiment is particularly important for understanding the biological response to synthetic materials *in vivo* as it is always a complex array of metabolites, lipids, and proteins that are associated with phenotypic changes. Ambient MSI techniques in particular are poised to see an increase in usage as there is no requirement for samples to be under vacuum, allowing the surface analysis of delicate substrates such as hydrogels and soft biomimetics – two substrates that are the foci of many emerging biomedical applications. The sampling probes used in many ambient MSI techniques are also very gentle, especially solvent-based methods such as nano-DESI, allowing the interrogation of delicate surfaces while leaving them physically unperturbed. Smart drug delivery systems comprise another emerging field of research, for example, nano- and micro-particles as drug carriers, in which SIMS imaging is uniquely capable to investigate, being able to monitor spatial distributions of inorganic particles within biological tissue as well as changes to select biomolecules within a single experiment, all at sub-micro spatial resolution. Further development of SIMS instrumentation and sample preparation including alternative primary-ion beams more amenable to detecting labile molecules intact, increased MS/MS capabilities, and development of metal- and matrix-enhanced SIMS[201,202] for increased sensitivity and cryogenic preparation/analysis will undoubtedly result in greater use of the technique, not only for biomaterials but for many other imaging applications. As for MALDI-MSI, due to its widespread popularity and strong commercial development for biological imaging applications we believe it is also well suited for biomaterials applications. Commercially available MALDI-MSI instrumentation is now able to provide a combination of both high spatial and mass resolution and major advancements are coming from increases in speed of acquisition and enhanced ionization methods. One notable advancement is the development of MALDI post-ionization that enables up to a two order of magnitude increase in sensitivity for certain molecules.[203] In addition, transmission geometry MALDI provides an avenue to increase spatial resolution to $\sim$1 μm for UV transparent subtrates.[204] Such resolution can enable, for example, studying molecular interactions between cells and materials at the subcellular level. Perhaps the largest disadvantage of MSI at the moment is the complications in acquiring quantitative MSI data, *i.e.*, absolute analyte quantities per unit area or volume. Such quantitative information is essential for many biomaterials applications yet is currently difficult to acquire with MSI. With careful experiment design, however, quantitative MSI data can be acquired and much progress has been made for this increasing in-demand capability over recent years through the development of various normalization strategies.[39]

In summary we strongly believe the MSI techniques outlined represent a diverse and useful set of tools for characterizing the molecular composition and responses of (bio)materials and they should see a growing usage in the biomaterials chemistry field in the near future.

Conflicts of interest

Gregory L. Fisher is an employee of Physical Electronics, Inc, a manufacturer and supplier of SIMS instruments.

Acknowledgements

This work was performed in the M4I research program financially supported by the Dutch Province of Limburg as part of the "LINK" program. This research received funding from the Netherlands Organization for Scientific Research (NWO) in the framework of the technology area COAST of the fund New Chemical Innovations. FMF acknowledges support from the American Society for Mass Spectrometry through a postdoctoral fellowship to MRLP, and from the National Science Foundation and the NASA Astrobiology Program, under the Center for Chemical Evolution (CHE-1504217).

References

1 A. M. Belu, D. J. Graham and D. G. Castner, *Biomaterials*, 2003, **24**, 3635–3653.
2 B. Ratner, A. Chilkoti and D. Castner, *Clin. Mater.*, 1992, **11**, 25–36.
3 M. López, J. Jiménez and A. Gutiérrez, *Vacuum*, 2011, **85**, 1076–1079.
4 K. D. Jandt, *Surf. Sci.*, 2001, **491**, 303–332.
5 J. Ong and L. Lucas, *Biomaterials*, 1998, **19**, 455–464.
6 K. L. Menzies and L. Jones, *Optom. Vis. Sci.*, 2010, **87**, 387–399.
7 P. Taddei, A. Tinti and G. Fini, *J. Raman Spectrosc.*, 2001, **32**, 619–629.
8 B. O. Leung, J. L. Brash and A. P. Hitchcock, *Materials*, 2010, **3**, 3911–3938.

9 K. Tsuji, K. Nakano, Y. Takahashi, K. Hayashi and C.-U. Ro, *Anal. Chem.*, 2012, **84**, 636–668.
10 M. Senoner and W. E. S. Unger, *J. Anal. At. Spectrom.*, 2012, **27**, 1050–1068.
11 A. Adriaens, L. Van Vaeck and F. Adams, *Mass Spectrom. Rev.*, 1999, **18**, 48–81.
12 A. C. Crecelius, J. Vitz and U. S. Schubert, *Anal. Chim. Acta*, 2014, **808**, 10–17.
13 A. Benninghoven, *Angew. Chem., Int. Ed. Engl.*, 1994, **33**, 1023–1043.
14 E. R. Amstalden van Hove, D. F. Smith and R. M. A. Heeren, *J. Chromatogr. A*, 2010, **1217**, 3946–3954.
15 A. Bodzon-Kulakowska, A. Drabik, J. Mystkowska, M. Chlabicz, M. Gacko, J. R. Dabrowski, P. Mielczarek, J. Silberring and P. Suder, *J. Biomed. Mater. Res., Part B*, 2016, **104**, 192–196.
16 M. Stoeckli, P. Chaurand, D. E. Hallahan and R. M. Caprioli, *Nat. Med.*, 2001, **7**, 493–496.
17 N. Winograd, *J. Biomol. Tech.: JBT*, 2012, **23**, S8.
18 Y. Cui, C. Bhardwaj, S. Milasinovic, R. P. Carlson, R. J. Gordon and L. Hanley, *ACS Appl. Mater. Interfaces*, 2013, **5**, 9269–9275.
19 R. F. K. Herzog and F. P. Viehböck, *Phys. Rev.*, 1949, **76**, 855–856.
20 R. M. A. Heeren, *Int. J. Mass Spectrom.*, 2015, **377**, 672–680.
21 J. C. Vickerman, *Analyst*, 1994, **119**, 513–523.
22 S. J. Pachuta and R. G. Cooks, *Chem. Rev.*, 1987, **87**, 647–669.
23 C. Lechene, F. Hillion, G. McMahon, D. Benson, A. M. Kleinfeld, J. P. Kampf, D. Distel, Y. Luyten, J. Bonventre, D. Hentschel, K. M. Park, S. Ito, M. Schwartz, G. Benichou and G. Slodzian, *J. Biol.*, 2006, **5**, 20.
24 G. Slodzian, B. Daigne, F. Girard, F. Boust and F. Hillion, *Biol. Cell.*, 1992, **74**, 43–50.
25 M. L. Kraft and H. A. Klitzing, *Biochim. Biophys. Acta*, 2014, **1841**, 1108–1119.
26 J. L. Guerquin-Kern, T. D. Wu, C. Quintana and A. Croisy, *Biochim. Biophys. Acta, Gen. Subj.*, 2005, **1724**, 228–238.
27 I. Lozic, R. V. Hartz, C. A. Bartlett, J. A. Shaw, M. Archer, P. S. Naidu, N. M. Smith, S. A. Dunlop, K. S. Iyer, M. R. Kilburn and M. Fitzgerald, *Biomaterials*, 2016, **74**, 200–216.
28 R. L. Wilson, J. F. Frisz, W. P. Hanafin, K. J. Carpenter, I. D. Hutcheon, P. K. Weber and M. L. Kraft, *Bioconjugate Chem.*, 2012, **23**, 450–460.
29 M. L. Steinhauser and C. P. Lechene, *Semin. Cell Dev. Biol.*, 2013, **24**, 661–667.
30 M. L. Steinhauser, A. P. Bailey, S. E. Senyo, C. Guillermier, T. S. Perlstein, A. P. Gould, R. T. Lee and C. P. Lechene, *Nature*, 2012, **481**, 516–519.
31 G. Enikolopov, C. Guillermier, M. Wang, L. Trakimas, M. L. Steinhauser and C. Lechene, *Surf. Interface Anal.*, 2014, **46**, 140–143.
32 S. E. Senyo, M. L. Steinhauser, C. L. Pizzimenti, V. K. Yang, L. Cai, M. Wang, T.-D. Wu, J.-L. Guerquin-Kern, C. P. Lechene and R. T. Lee, *Nature*, 2013, **493**, 433–436.
33 C. Scharlach, L. Müller, S. Wagner, Y. Kobayashi, H. Kratz, M. Ebert, N. Jakubowski and E. Schellenberger, *J. Biomed. Nanotechnol.*, 2016, **12**, 1001–1010.
34 S. G. Elci, B. Yan, S. T. Kim, K. Saha, Y. Jiang, G. A. Klemmer, D. F. Moyano, G. Y. Tonga, V. M. Rotello and R. W. Vachet, *Analyst*, 2016, **141**, 2418–2425.
35 F. Amerstorfer, S. Fischerauer, L. Fischer, J. Eichler, J. Draxler, A. Zitek, M. Meischel, E. Martinelli, T. Kraus and S. Hann, *Acta Biomater.*, 2016, **42**, 440–450.
36 J. Draxler, E. Martinelli, A. M. Weinberg, A. Zitek, J. Irrgeher, M. Meischel, S. E. Stanzl-Tschegg, B. Mingler and T. Prohaska, *Acta Biomater.*, 2017, **51**, 526–536.
37 M. Meischel, D. Hörmann, J. Draxler, E. K. Tschegg, J. Eichler, T. Prohaska and S. E. Stanzl-Tschegg, *J. Mech. Behav. Biomed. Mater.*, 2017, **71**, 307–313.
38 M. V. Zoriy and J. S. Becker, *Int. J. Mass spectrom.*, 2007, **264**, 175–180.
39 S. R. Ellis, A. L. Bruinen and R. M. A. Heeren, *Anal. Bioanal. Chem.*, 2014, **406**, 1275–1289.
40 D. Pozebon, G. Scheffler and V. Dressler, *J. Anal. At. Spectrom.*, 2017, **32**, 890–919.
41 M. K. Passarelli and N. Winograd, *Biochim. Biophys. Acta*, 2011, **1811**, 976–990.
42 N. Winograd, *Anal. Chem.*, 2015, **87**, 328–333.
43 D. Weibel, N. Lockyer and J. Vickerman, *Appl. Surf. Sci.*, 2004, **231**, 146–152.
44 N. Winograd, *Anal. Chem.*, 2005, **77**, 142–149.
45 D. Weibel, S. Wong, N. Lockyer, P. Blenkinsopp, R. Hill and J. C. Vickerman, *Anal. Chem.*, 2003, **75**, 1754–1764.
46 J. Cheng, J. Kozole, R. Hengstebeck and N. Winograd, *J. Am. Soc. Mass Spectrom.*, 2007, **18**, 406–412.
47 E. A. Jones, N. P. Lockyer and J. C. Vickerman, *Int. J. Mass spectrom.*, 2007, **260**, 146–157.
48 G. Gillen, M. Walker, P. Thompson and J. Bennett, *J. Vac. Sci. Technol., B: Microelectron. Nanometer Struct.–Process., Meas., Phenom.*, 2000, **18**, 503–508.
49 E. R. Fuoco, G. Gillen, M. B. J. Wijesundara, W. E. Wallace and L. Hanley, *J. Phys. Chem. B*, 2001, **105**, 3950–3956.
50 A. D. Appelhans and J. E. Delmore, *Anal. Chem.*, 1989, **61**, 1087–1093.
51 N. Davies, D. E. Weibel, P. Blenkinsopp, N. Lockyer, R. Hill and J. C. Vickerman, *Appl. Surf. Sci.*, 2003, **203–204**, 223–227.
52 D. Touboul, F. Kollmer, E. Niehuis, A. Brunelle and O. Laprévote, *J. Am. Soc. Mass Spectrom.*, 2005, **16**, 1608–1618.
53 Z. Li, S. V. Verkhoturov and E. A. Schweikert, *Anal. Chem.*, 2006, **78**, 7410–7416.
54 S. Rabbani, A. M. Barber, J. S. Fletcher, N. P. Lockyer and J. C. Vickerman, *Anal. Chem.*, 2011, **83**, 3793–3800.
55 S. Ninomiya, Y. Nakata, Y. Honda, K. Ichiki, T. Seki, T. Aoki and J. Matsuo, *Appl. Surf. Sci.*, 2008, **255**, 1588–1590.
56 N. Toyoda, J. Matsuo, T. Aoki, I. Yamada and D. B. Fenner, *Appl. Surf. Sci.*, 2003, **203**, 214–218.
57 H. Tian, L. Sparvero, A. A. Amoscato, V. Kagan, H. Bayir and N. Winograd, Indianapolis, 2017.

58 S. Sheraz née Rabbani, A. Barber, J. S. Fletcher, N. P. Lockyer and J. C. Vickerman, *Anal. Chem.*, 2013, **85**, 5654–5658.
59 Z. Postawa, B. Czerwinski, M. Szewczyk, E. J. Smiley, N. Winograd and B. J. Garrison, *Anal. Chem.*, 2003, **75**, 4402–4407.
60 H. Tian, L. Sparvero, A. A. Amoscato, V. Kagan, H. Bayir and N. Winograd, ASMS 2017 Indianapolis, 2017.
61 H. Tian, D. A. Six, T. Krucker, J. A. Leeds and N. Winograd, *Anal. Chem.*, 2017, **89**, 5050–5057.
62 J. S. Fletcher, N. P. Lockyer and J. C. Vickerman, *Mass Spectrom. Rev.*, 2011, **30**, 142–174.
63 A. Wucher, G. L. Fisher and C. M. Mahoney, *Cluster Secondary Ion Mass Spectrometry*, John Wiley & Sons, Inc., 2013, ch. 6, pp. 207–246, DOI: 10.1002/9781118589335.
64 E. Niehuis, R. Moellers, D. Rading and P. Bruener, *Surf. Interface Anal.*, 2014, **46**, 70–73.
65 A. Wucher, J. Cheng, L. Zheng and N. Winograd, *Anal. Bioanal. Chem.*, 2009, **393**, 1835–1842.
66 C. Bich, D. Touboul and A. Brunelle, *Mass Spectrom. Rev.*, 2014, **33**, 442–451.
67 C. Bich, D. Touboul and A. Brunelle, *Biointerphases*, 2015, **10**, 7.
68 N. Winograd and B. J. Garrison, *Annu. Rev. Phys. Chem.*, 2010, **61**, 305–322.
69 J. Fletcher and J. Vickerman, *Anal. Bioanal. Chem.*, 2010, **396**, 85–104.
70 K. Chughtai and R. M. A. Heeren, *Chem. Rev.*, 2010, **110**, 3237–3277.
71 D. Touboul, O. Laprevote and A. Brunelle, *Curr. Opin. Chem. Biol.*, 2011, **15**, 725–732.
72 E. J. Lanni, S. S. Rubakhin and J. V. Sweedler, *J. Proteomics*, 2012, **75**, 5036–5051.
73 N. P. Lockyer, *Methods Mol. Biol.*, 2014, **1117**, 707–732.
74 J. Yang and I. Gilmore, *Mater. Sci. Technol.*, 2015, **31**, 131–136.
75 M. K. Passarelli and A. G. Ewing, *Curr. Opin. Chem. Biol.*, 2013, **17**, 854–859.
76 C. M. Mahoney, *Mass Spectrom. Rev.*, 2010, **29**, 247–293.
77 H. W. Werner, *Surf. Sci.*, 1975, **47**, 301–323.
78 H. W. Werner and H. van der Wel, *Anal. Methods Instrum.*, 1995, **2**, 111–121.
79 J. Bailey, R. Havelund, A. G. Shard, I. S. Gilmore, M. R. Alexander, J. S. Sharp and D. J. Scurr, *ACS Appl. Mater. Interfaces*, 2015, **7**, 2654–2659.
80 T. Mouhib, A. Delcorte, C. Poleunis and P. Bertrand, *Surf. Interface Anal.*, 2011, **43**, 175–178.
81 X. Ren, L.-T. Weng, C.-M. Chan and K.-M. Ng, *Anal. Chem.*, 2012, **84**, 8497–8504.
82 I. F. Patel, M. V. Kiryukhin, N. L. Yakovlev, H. S. Gupta and G. B. Sukhorukov, *J. Mater. Chem. B*, 2015, **3**, 4821–4830.
83 S. Jung, M. Foston, U. C. Kalluri, G. A. Tuskan and A. J. Ragauskas, *Angew. Chem., Int. Ed.*, 2012, **51**, 12005–12008.
84 O. J. G. M. Goor, H. M. Keizer, A. L. Bruinen, M. G. J. Schmitz, R. M. Versteegen, H. M. Janssen, R. M. A. Heeren and P. Y. W. Dankers, *Adv. Mater.*, 2017, **29**, 1604652.
85 S. Wang, J. Lv, J. Ma and S. Zhang, *Nanotoxicology*, 2016, **10**, 1129–1135.
86 F. Kollmer, W. Paul, M. Krehl and E. Niehuis, *Surf. Interface Anal.*, 2013, **45**, 312–314.
87 B. Hagenhoff, D. Breitenstein, E. Tallarek, R. Möllers, E. Niehuis, M. Sperber, B. Goricnik and J. Wegener, *Surf. Interface Anal.*, 2013, **45**, 315–319.
88 T. B. Angerer and J. S. Fletcher, *Surf. Interface Anal.*, 2014, **46**, 198–203.
89 J. Kokesch-Himmelreich, B. Woltmann, B. Torger, M. Rohnke, S. Arnhold, U. Hempel, M. Müller and J. Janek, *Anal. Bioanal. Chem.*, 2015, **407**, 4555–4565.
90 F. P. Y. Barré, R. M. A. Heeren and N. Ogrinc Potočnik, *Curr. Pharm. Des.*, 2017, **23**, 1–11.
91 D. R. Baer, D. J. Gaspar, P. Nachimuthu, S. D. Techane and D. G. Castner, *Anal. Bioanal. Chem.*, 2010, **396**, 983–1002.
92 H. E. Townley, J. Kim and P. J. Dobson, *Nanoscale*, 2012, **4**, 5043–5050.
93 I. R. Fernando, D. P. Ferris, M. Frasconi, D. Malin, E. Strekalova, M. D. Yilmaz, M. W. Ambrogio, M. M. Algaradah, M. P. Hong, X. Chen, M. S. Nassar, Y. Y. Botros, V. L. Cryns and J. F. Stoddart, *Nanoscale*, 2015, **7**, 7178–7183.
94 J. W. Moreau, P. K. Weber, M. C. Martin, B. Gilbert, I. D. Hutcheon and J. F. Banfield, *Science*, 2007, **316**, 1600–1603.
95 J.-P. Piret, D. Jacques, J.-N. Audinot, J. Mejia, E. Boilan, F. Noel, M. Fransolet, C. Demazy, S. Lucas, C. Saout and O. Toussaint, *Nanoscale*, 2012, **4**, 7168–7184.
96 Y. P. Kim, H. K. Shon, S. K. Shin and T. G. Lee, *Mass Spectrom. Rev.*, 2015, **34**, 237–247.
97 X. Hua, C. Szymanski, Z. Wang, Y. Zhou, X. Ma, J. Yu, J. Evans, G. Orr, S. Liu, Z. Zhu and X.-Y. Yu, *Integr. Biol.*, 2016, **8**, 635–644.
98 A. Rafati, A. Boussahel, K. M. Shakesheff, A. G. Shard, C. J. Roberts, X. Chen, D. J. Scurr, S. Rigby-Singleton, P. Whiteside, M. R. Alexander and M. C. Davies, *J. Controlled Release*, 2012, **162**, 321–329.
99 C.-Y. Lee, G. M. Harbers, D. W. Grainger, L. J. Gamble and D. G. Castner, *J. Am. Chem. Soc.*, 2007, **129**, 9429–9438.
100 H. K. Shon, J. Park, I. Choi, H. M. Park, D. W. Moon and T. G. Lee, *J. Nanosci. Nanotechnol.*, 2011, **11**, 638–641.
101 D. J. Graham, J. T. Wilson, J. J. Lai, P. S. Stayton and D. G. Castner, *Biointerphases*, 2016, **11**, 02A304.
102 M. T. Proetto, C. R. Anderton, D. Hu, C. J. Szymanski, Z. Zhu, J. P. Patterson, J. K. Kammeyer, L. G. Nilewski, A. M. Rush, N. C. Bell, J. E. Evans, G. Orr, S. B. Howell and N. C. Gianneschi, *ACS Nano*, 2016, **10**, 4046–4054.
103 C. A. Barnes, J. Brison, M. Robinson, D. J. Graham, D. G. Castner and B. D. Ratner, *Anal. Chem.*, 2012, **84**, 893–900.
104 N. Georgi, B. Cillero-Pastor, G. B. Eijkel, P. C. Periyasamy, A. Kiss, C. van Blitterswijk, J. N. Post, R. M. Heeren and M. Karperien, *Anal. Chem.*, 2015, **87**, 3981–3988.
105 G. M. de Peppo, P. Sjovall, M. Lennerås, R. Strehl, J. Hyllner, P. Thomsen and C. Karlsson, *Tissue Eng., Part A*, 2010, **16**, 3413–3426.

106 G. M. de Peppo, M. Sladkova, P. Sjovall, A. Palmquist, K. Oudina, J. Hyllner, P. Thomsen, H. Petite and C. Karlsson, *Tissue Eng., Part A*, 2013, **19**, 175–187.

107 A. Chilkoti, A. E. Schmierer, V. Perezluna and B. D. Ratner, *Anal. Chem.*, 1995, **67**, 2883–2891.

108 Y. Mei, K. Saha, S. R. Bogatyrev, J. Yang, A. L. Hook, Z. I. Kalcioglu, S. W. Cho, M. Mitalipova, N. Pyzocha, F. Rojas, K. J. Van Vliet, M. C. Davies, M. R. Alexander, R. Langer, R. Jaenisch and D. G. Anderson, *Nat. Mater.*, 2010, **9**, 768–778.

109 K. Saha, Y. Mei, C. M. Reisterer, N. K. Pyzocha, J. Yang, J. Muffat, M. C. Davies, M. R. Alexander, R. Langer, D. G. Anderson and R. Jaenisch, *Proc. Natl. Acad. Sci. U. S. A.*, 2011, **108**, 18714–18719.

110 D. Pasqui, P. Torricelli, M. De Cagna, M. Fini and R. Barbucci, *J. Biomed. Mater. Res., Part A*, 2014, **102**, 1568–1579.

111 T. A. Ulrich, T. G. Lee, H. K. Shon, D. W. Moon and S. Kumar, *Biomaterials*, 2011, **32**, 5633–5642.

112 J. A. DeQuach, V. Mezzano, A. Miglani, S. Lange, G. M. Keller, F. Sheikh and K. L. Christman, *PLoS One*, 2010, **5**, e13039.

113 B. N. Brown, C. A. Barnes, R. T. Kasick, R. Michel, T. W. Gilbert, D. Beer-Stolz, D. G. Castner, B. D. Ratner and S. F. Badylak, *Biomaterials*, 2010, **31**, 428–437.

114 C. A. Barnes, J. Brison, R. Michel, B. N. Brown, D. G. Castner, S. F. Badylak and B. D. Ratner, *Biomaterials*, 2011, **32**, 137–143.

115 J. Park, S. Bauer, A. Pittrof, M. S. Killian, P. Schmuki and K. von der Mark, *Small*, 2012, **8**, 98–107.

116 M. Bongo, O. Winther-Jensen, S. Himmelberger, X. Strakosas, M. Ramuz, A. Hama, E. Stavrinidou, G. G. Malliaras, A. Salleo, B. Winther-Jensen and R. M. Owens, *J. Mater. Chem. B*, 2013, **1**, 3860–3867.

117 A. R. Lodding, P. M. Fischer, H. Odelius, J. G. Norén, L. Sennerby, C. B. Johansson, J. M. Chabala and R. Levi-Setti, *Anal. Chim. Acta*, 1990, **241**, 299–314.

118 C. Eriksson, P. Malmberg and H. Nygren, *Rapid Commun. Mass Spectrom.*, 2008, **22**, 943–949.

119 M. Gonzalez, E. Salvagni, J. C. Rodriguez-Cabello, E. Ruperez, F. J. Gil, J. Pena and J. M. Manero, *J. Biomed. Mater. Res., Part A*, 2013, **101**, 819–826.

120 G. L. Fisher, A. M. Belu, C. M. Mahoney, K. Wormuth and N. Sanada, *Anal. Chem.*, 2009, **81**, 9930–9940.

121 L. A. Klerk, P. Y. Dankers, E. R. Popa, A. W. Bosman, M. E. Sanders, K. A. Reedquist and R. M. Heeren, *Anal. Chem.*, 2010, **82**, 4337–4343.

122 J. S. Fletcher, S. Rabbani, A. Henderson, P. Blenkinsopp, S. P. Thompson, N. P. Lockyer and J. C. Vickerman, *Anal. Chem.*, 2008, **80**, 9058–9064.

123 R. Hill, P. Blenkinsopp, S. Thompson, J. Vickerman and J. S. Fletcher, *Surf. Interface Anal.*, 2011, **43**, 506–509.

124 A. Carado, M. K. Passarelli, J. Kozole, J. E. Wingate, N. Winograd and A. V. Loboda, *Anal. Chem.*, 2008, **80**, 7921–7929.

125 G. L. Fisher, A. L. Bruinen, N. Ogrinc Potočnik, J. S. Hammond, S. R. Bryan, P. E. Larson and R. M. A. Heeren, *Anal. Chem.*, 2016, **88**, 6433–6440.

126 A. Carado, J. Kozole, M. Passarelli, N. Winograd, A. Loboda, J. Bunch, J. Wingate, J. Hankin and R. Murphy, *Appl. Surf. Sci.*, 2008, **255**, 1572–1575.

127 G. L. Fisher, J. S. Hammond, P. E. Larson, S. R. Bryan and R. M. Heeren, *J. Vac. Sci. Technol., B*, 2016, **34**, 03H126.

128 G. L. Fisher, J. S. Hammond, S. R. Bryan, P. E. Larson and R. M. A. Heeren, *Microsc. Microanal.*, 2017, 1–6, DOI: 10.1017/S1431927617000654.

129 D. F. Smith, A. Kiss, F. E. Leach, E. W. Robinson, L. Paša-Tolić and R. M. A. Heeren, *Anal. Bioanal. Chem.*, 2013, **405**, 6069–6076.

130 J. D. DeBord, D. F. Smith, C. R. Anderton, R. M. A. Heeren, L. Paša-Tolić, R. H. Gomer and F. A. Fernandez-Lima, *PLoS One*, 2014, **9**, e99319.

131 A. Pirkl, R. Möllers, E. Niehuis, M. K. Passarelli, A. Makarov, S. Horning and I. S. Gilmore, *Front. Bioeng. Biotechnol.*, 10th World Biomaterials Congress, Montreal, Canada, 2016, DOI: 10.3389/conf.FBIOE.2016.01.00785.

132 M. Karas, D. Bachmann and F. Hillenkamp, *Anal. Chem.*, 1985, **57**, 2935–2939.

133 M. Karas, D. Bachmann, U. Bahr and F. Hillenkamp, *Int. J. Mass Spectrom. Ion Processes*, 1987, **78**, 53–68.

134 K. Tanaka, H. Waki, Y. Ido, S. Akita, Y. Yoshida, T. Yoshida and T. Matsuo, *Rapid Commun. Mass Spectrom.*, 1988, **2**, 151–153.

135 A. Dass, A. Stevenson, G. R. Dubay, J. B. Tracy and R. W. Murray, *J. Am. Chem. Soc.*, 2008, **130**, 5940–5946.

136 N. C. Dopke, P. M. Treichel and M. M. Vestling, *Inorg. Chem.*, 1998, **37**, 1272–1277.

137 C. Y. Shi and C. H. Deng, *Analyst*, 2016, **141**, 2816–2826.

138 V. V. Laiko, M. A. Baldwin and A. L. Burlingame, *Anal. Chem.*, 2000, **72**, 652–657.

139 A. Römpp and B. Spengler, *Histochem. Cell Biol.*, 2013, **139**, 759–783.

140 R. M. A. Heeren, L. A. McDonnell, E. Amstalden, S. L. Luxembourg, A. F. M. Altelaar and S. R. Piersma, *Appl. Surf. Sci.*, 2006, **252**, 6827–6835.

141 L. MacAleese, M. C. Duursma, L. A. Klerk, G. Fisher and R. M. A. Heeren, *J. Proteomics*, 2011, **74**, 993–1001.

142 R. M. Caprioli, T. B. Farmer and J. Gile, *Anal. Chem.*, 1997, **69**, 4751–4760.

143 K. Schwamborn and R. M. Caprioli, *Nat. Rev. Cancer*, 2010, **10**, 639–646.

144 K. A. Zemski Berry, J. A. Hankin, R. M. Barkley, J. M. Spraggins, R. M. Caprioli and R. C. Murphy, *Chem. Rev.*, 2011, **111**, 6491–6512.

145 L. A. McDonnell and R. M. A. Heeren, *Mass Spectrom. Rev.*, 2007, **26**, 606–643.

146 N. Ogrinc Potočnik, T. Porta, M. Becker, R. M. A. Heeren and S. R. Ellis, *Rapid Commun. Mass Spectrom.*, 2015, **29**, 2195–2203.

147 A. Zavalin, J. Yang, K. Hayden, M. Vestal and R. M. Caprioli, *Anal. Bioanal. Chem.*, 2015, **407**, 2337–2342.

148 M. Kompauer, S. Heiles and B. Spengler, *Nat. Methods*, 2017, **14**, 90–96.

149 R. D. Addie, B. Balluff, J. V. M. G. Bovée, H. Morreau and L. A. McDonnell, *Anal. Chem.*, 2015, **87**, 6426–6433.

150 A. C. Crecelius, T. Alexandrov and U. S. Schubert, *Rapid Commun. Mass Spectrom.*, 2011, **25**, 2809–2814.
151 A. C. Crecelius, R. Steinacker, A. Meier, T. Alexandrov, J. Vitz and U. S. Schubert, *Anal. Chem.*, 2012, **84**, 6921–6925.
152 D. Rivas, A. Ginebreda, S. Pérez, C. Quero and D. Barceló, *Sci. Total Environ.*, 2016, **566–567**, 27–33.
153 M. Kurth, P. Eyerer, R. Ascherl, K. Dittel and U. Holz, *J. Biomater. Appl.*, 1988, **3**, 33–51.
154 P. Eyerer, M. Kurth, H. A. McKellup and T. Mittlmeier, *J. Biomed. Mater. Res.*, 1987, **21**, 275–291.
155 S. M. Fröhlich, V. Dorrer, V.-M. Archodoulaki, G. Allmaier and M. Marchetti-Deschmann, *EuPa Open Proteomics*, 2014, **4**, 70–80.
156 H. Bergmeister, N. Seyidova, C. Schreiber, M. Strobl, C. Grasl, I. Walter, B. Messner, S. Baudis, S. Fröhlich, M. Marchetti-Deschmann, M. Griesser, M. di Franco, M. Krssak, R. Liska and H. Schima, *Acta Biomater.*, 2015, **11**, 104–113.
157 S. M. Frohlich, M. Eilenberg, A. Svirkova, C. Grasl, R. Liska, H. Bergmeister and M. Marchetti-Deschmann, *Analyst*, 2015, **140**, 6089–6099.
158 K. Medini, B. West, D. E. Williams, M. A. Brimble and J. A. Gerrard, *Chem. Commun.*, 2017, **53**, 1715–1718.
159 S. Chen, C. Xiong, H. Liu, Q. Wan, J. Hou, Q. He, A. Badu-Tawiah and Z. Nie, *Nat. Nanotechnol.*, 2015, **10**, 176–182.
160 B. Creran, B. Yan, D. F. Moyano, M. M. Gilbert, R. W. Vachet and V. M. Rotello, *Chem. Commun.*, 2012, **48**, 4543–4545.
161 R. G. Cooks, Z. Ouyang, Z. Takats and J. M. Wiseman, *Science*, 2006, **311**, 1566–1570.
162 D. J. Weston, *Analyst*, 2010, **135**, 661–668.
163 G. A. Harris, A. S. Galhena and F. M. Fernandez, *Anal. Chem.*, 2011, **83**, 4508–4538.
164 C. Wu, A. L. Dill, L. S. Eberlin, R. G. Cooks and D. R. Ifa, *Mass Spectrom. Rev.*, 2013, **32**, 218–243.
165 M. R. L. Paine, P. J. Barker and S. J. Blanksby, *Anal. Chim. Acta*, 2014, **808**, 70–82.
166 M. E. Monge, G. A. Harris, P. Dwivedi and F. M. Fernández, *Chem. Rev.*, 2013, **113**, 2269–2308.
167 P. Nemes and A. Vertes, *TrAC, Trends Anal. Chem.*, 2012, **34**, 22–34.
168 M.-Z. Huang, C.-H. Yuan, S.-C. Cheng, Y.-T. Cho and J. Shiea, *Annu. Rev. Anal. Chem.*, 2010, **3**, 43–65.
169 J. Laskin and I. Lanekoff, *Anal. Chem.*, 2016, **88**, 52–73.
170 A. Venter, P. E. Sojka and R. G. Cooks, *Anal. Chem.*, 2006, **78**, 8549–8555.
171 V. Kertesz, G. J. Van Berkel, M. Vavrek, K. A. Koeplinger, B. B. Schneider and T. R. Covey, *Anal. Chem.*, 2008, **80**, 5168–5177.
172 V. Kertesz and G. J. Van Berkel, *Anal. Chem.*, 2008, **80**, 1027–1032.
173 V. Kertesz and G. J. Van Berkel, *Rapid Commun. Mass Spectrom.*, 2008, **22**, 2639–2644.
174 S. M. Reiter, W. Buchberger and C. W. Klampfl, *Anal. Bioanal. Chem.*, 2010, **400**, 2317–2322.
175 C. Wu, A. L. Dill, L. S. Eberlin, R. G. Cooks and D. R. Ifa, *Mass Spectrom. Rev.*, 2012, **32**, 218–243.
176 R. V. Bennett, H. J. Cleaves, J. M. Davis, D. A. Sokolov, T. M. Orlando, J. L. Bada and F. M. Fernández, *Anal. Chem.*, 2013, **85**, 1276–1279.
177 M. R. L. Paine, P. J. Barker and S. J. Blanksby, *Analyst*, 2011, **136**, 904–912.
178 A. Bodzon-Kulakowska, A. Drabik, J. Mystkowska, M. Chlabicz, M. Gacko, J. R. Dabrowski, P. Mielczarek, J. Silberring and P. Suder, *J. Biomed. Mater. Res., Part B*, 2016, **104**, 192–196.
179 G. J. Van Berkel, A. D. Sanchez and J. M. E. Quirke, *Anal. Chem.*, 2002, **74**, 6216–6223.
180 G. J. Van Berkel and V. Kertesz, *Anal. Chem.*, 2006, **78**, 4938–4944.
181 G. J. Van Berkel, V. Kertesz, K. A. Koeplinger, M. Vavrek and A.-N. T. Kong, *J. Mass Spectrom.*, 2008, **43**, 500–508.
182 M. S. ElNaggar, B. Prideaux, V. Dartois and J. M. Wiseman, *Curr. Metabolomics*, 2014, **2**, 122–131.
183 C.-C. Hsu, M. S. ElNaggar, Y. Peng, J. Fang, L. M. Sanchez, S. J. Mascuch, K. A. Møller, E. K. Alazzeh, J. Pikula, R. A. Quinn, Y. Zeng, B. E. Wolfe, R. J. Dutton, L. Gerwick, L. Zhang, X. Liu, M. Månsson and P. C. Dorrestein, *Anal. Chem.*, 2013, **85**, 7014–7018.
184 D. Eikel and J. Henion, *Rapid Commun. Mass Spectrom.*, 2011, **25**, 2345–2354.
185 M. R. L. Paine, P. J. Barker, S. A. Maclauglin, T. W. Mitchell and S. J. Blanksby, *Rapid Commun. Mass Spectrom.*, 2012, **26**, 412–418.
186 D. Eikel, M. Vavrek, S. Smith, C. Bason, S. Yeh, W. A. Korfmacher and J. D. Henion, *Rapid Commun. Mass Spectrom.*, 2011, **25**, 3587–3596.
187 L. Tomlinson, J. Fuchser, A. Fütterer, M. Baumert, D. G. Hassall, A. West and P. S. Marshall, *Rapid Commun. Mass Spectrom.*, 2014, **28**, 995–1003.
188 S. H. J. Brown, L. H. Huxtable, M. D. P. Willcox, S. J. Blanksby and T. W. Mitchell, *Analyst*, 2013, **138**, 1316–1320.
189 P. Nemes and A. Vertes, *Anal. Chem.*, 2007, **79**, 8098–8106.
190 J. Shiea, M.-Z. Huang, H.-J. Hsu, C.-Y. Lee, C.-H. Yuan, I. Beech and J. Sunner, *Rapid Commun. Mass Spectrom.*, 2005, **19**, 3701–3704.
191 E. J. Judge, J. J. Brady, D. Dalton and R. J. Levis, *Anal. Chem.*, 2010, **82**, 3231–3238.
192 P. Nemes, A. A. Barton and A. Vertes, *Anal. Chem.*, 2009, **81**, 6668–6675.
193 S.-Y. Lin, M.-Z. Huang, H.-C. Chang and J. Shiea, *Anal. Chem.*, 2007, **79**, 8789–8795.
194 O. S. Ovchinnikova, M. Lorenz, V. Kertesz and G. J. Van Berkel, *Anal. Chem.*, 2013, **85**, 10211–10217.
195 O. S. Ovchinnikova and G. J. Van Berkel, *Rapid Commun. Mass Spectrom.*, 2010, **24**, 1721–1729.
196 O. S. Ovchinnikova, V. Kertesz and G. J. Van Berkel, *Anal. Chem.*, 2011, **83**, 598–603.
197 S. Jesse, R. K. Vasudevan, L. Collins, E. Strelcov, M. B. Okatan, A. Belianinov, A. P. Baddorf, R. Proksch

and S. V. Kalinin, *Annu. Rev. Phys. Chem.*, 2014, **65**, 519–536.
198 O. S. Ovchinnikova, M. P. Nikiforov, J. A. Bradshaw, S. Jesse and G. J. Van Berkel, *ACS Nano*, 2011, **5**, 5526–5531.
199 O. S. Ovchinnikova, K. Kjoller, G. B. Hurst, D. A. Pelletier and G. J. Van Berkel, *Anal. Chem.*, 2014, **86**, 1083–1090.
200 O. S. Ovchinnikova, T. Tai, V. Bocharova, M. B. Okatan, A. Belianinov, V. Kertesz, S. Jesse and G. J. Van Berkel, *ACS Nano*, 2015, **9**, 4260–4269.
201 A. F. M. Altelaar, I. Klinkert, K. Jalink, R. P. J. de Lange, R. A. H. Adan, R. M. A. Heeren and S. R. Piersma, *Anal. Chem.*, 2006, **78**, 734–742.
202 F. N. Svara, A. Kiss, T. W. Jaskolla, M. Karas and R. M. A. Heeren, *Anal. Chem.*, 2011, **83**, 8308–8313.
203 J. Soltwisch, H. Kettling, S. Vens-Cappell, M. Wiegelmann, J. Müthing and K. Dreisewerd, *Science*, 2015, **348**, 211.
204 A. Zavalin, E. M. Todd, P. D. Rawhouser, J. Yang, J. L. Norris and R. M. Caprioli, *J. Mass Spectrom.*, 2012, **47**, i.

